

Spin Nernst effect in the absence of a magnetic field

Xuele Liu¹ and X.C. Xie^{1,2}

¹*Department of Physics, Oklahoma State University, Stillwater, Oklahoma 74078*

²*Institute of Physics, Chinese Academy of Sciences, Beijing 100190, China*

We study the spin Nernst effect of a mesoscopic four-terminal cross-bar device with the Rashba spin-orbit interaction (SOI) in the absence of a magnetic field. The interplay between the spin Nernst effect and the seebeck coefficient is investigated for a wide range of the Rashba SOI. When no peaks appeared in the seebeck coefficient, an oscillatory spin Nernst effect still occurs. In addition, the disorder effect on the spin Nernst effect is also studied. We find that the spin Nernst effect can be enhanced up to three-fold by disorder. Besides, due to the interface effect, the counter-propagating of the charge current to the direction of the temperature gradient is possible for a nonuniform system.

PACS numbers: 72.15.Jf, 72.25.-b, 73.23.-b, 73.43.-f

Keywords: A. Rashba spin-orbit interaction; C. Disorder; D. Spin Nernst Effect; D. seebeck coefficient

With the development of the micro-fabrication technology and the low-temperature measurement technology, a great amount of efforts have been paid for the research of the thermoelectric properties in the last two decades^{2,3}. Comparing to the conductance, the thermoelectric coefficients of electronic systems are more sensitive to the details of the density of states⁴⁻⁶, which is very important for the design of the electronic devices. The thermopower (seebeck coefficient) of the quantum dot was measured in the last few years². Recently, the Nernst effect, a Hall-like thermal effect, has been theoretically studied⁷ and had been detected, for example, in bismuth⁸ in which, with the existence of a perpendicular magnetic field, a transverse current is induced by the longitudinal thermal gradient.

In the spintronics area, the spin thermal coefficients are also of focus recently⁴⁻⁶. In a recent paper, by considering a system with a spin-orbit interaction (SOI), the Nernst effect and a novel thermal effect, the spin Nernst effect, have been fully studied in a two-dimensional electron gas⁹. It is found that, because of a perpendicular magnetic field B , the Nernst signal exhibits a series of peaks. When the SOI exists, the peaks split and the spin Nernst effect appears. With a small B or a large SOI, the spin Nernst effect becomes more pronounced. It also shows that the spin Nernst effect is easier to be affected by disorder than the Nernst effect.

There is no doubt that a perpendicular magnetic field B is essential for the existence of the Nernst effect. However, in the spin Hall effect, the transverse spin current is due to a SOI rather than a perpendicular magnetic field. Similarly, for the spin Nernst effect, B may not be needed either. One may suspect that the spin Nernst effect is in fact the combination of the existence of thermopower and a SOI. Thus, the focus of the current work is to study the spin Nernst effect in the absence of a perpendicular magnetic field, and its interplay with the thermopower.

In this paper, the property of spin Nernst effect is developed in a two-dimensional electron gas system with a Rashba SOI but without a perpendicular magnetic field B . For this set-up, the Nernst effect disappears thus we

focus on the spin Nernst effect – a transverse spin current induced by a longitudinal thermal gradient $\Delta\mathcal{T}$. A traditional way to analyze such a Hall-like system is to add vertical probes to detect the transverse properties. Thus we set a four-terminal cross-bar sample, as shown in Fig.1⁹. A longitudinal thermal gradient $\Delta\mathcal{T}$ is added between the leads 1 and 3. This thermal gradient induces a transverse spin current J_s in the closed boundary condition with a SOI, which can be measured at leads 2 and 4. The seebeck coefficient of such a system can be directly measured at leads 1 and 3.

By using a tight-binding model and the Landauer-Buttiker (LB) formula, the spin Nernst coefficient N_s ($N_s \equiv J_s/\Delta\mathcal{T}$) and the seebeck coefficient S ($S \equiv -\Delta V/\Delta\mathcal{T}$) are calculated. The Rashba SOI used in our calculations covers a wide range with some beyond the accessibility of today's sample. The seebeck coefficient S shows a few peaks consequently when the fermi energy E_F goes through the energy band. Due to the interface of our setting (zero Rashba SOI at lead 2,4), we find a negative S . It is confirmed that spin Nernst effect can not be simply thought as the combination of the seebeck coefficient and the Spin hall effect⁹. A big spin Nernst coefficient N_s can be found with a zero seebeck coefficient S . However, when the peaks of seebeck coefficient occur with a non-zero Rashba SOI, the spin Nernst effect exhibits big amplitude or sometimes also peaks. The Fermi energy E_F also affects N_s . When the Fermi energy E_F is close to the bottom of the energy band ($-4t$), the oscillatory amplitude of N_s becomes more pronounced. The effect of disorder on N_s is also investigated. When $E_F = -3.8t$, we can see a large increase of N_s with increasing of the strength of disorder. Its value at the peak is about three-fold of that without disorder. In addition, we find that the strength of disorder when N_s vanishes, indicating that the system goes into an insulating regime, is independent of the Fermi energy.

In the tight-binding representation, the Hamiltonian

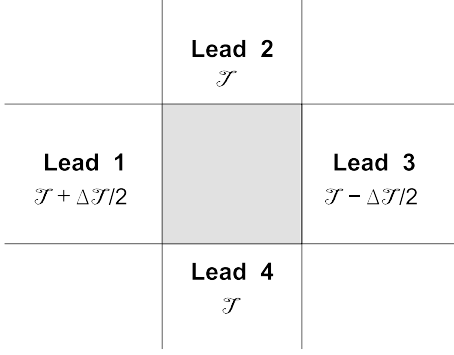


FIG. 1: Schematic diagram of the four-terminal cross-bar sample. The area with SOI is marked by gray. A thermal gradient $\Delta\mathcal{T}$ is applied between the longitudinal lead-1 and lead-3.

with SOI can be written as:¹⁰,

$$H = \sum_{\mathbf{i}\sigma} \varepsilon_{\mathbf{i}} c_{\mathbf{i}\sigma}^\dagger c_{\mathbf{i}\sigma} + \sum_{\mathbf{i}\sigma\sigma'} [c_{\mathbf{i}+\delta y, \sigma}^\dagger (-t\mathbf{I} - i\sigma_x V_R)_{\sigma\sigma'} c_{\mathbf{i}\sigma'} + c_{\mathbf{i}+\delta x, \sigma}^\dagger (-t\mathbf{I} + i\sigma_y V_R)_{\sigma\sigma'} c_{\mathbf{i}\sigma'} + H.c.] \quad (1)$$

where $c_{\mathbf{i}\sigma}^\dagger$ ($c_{\mathbf{i}\sigma}$) is the creation (annihilation) operator of electrons in the site $\mathbf{i} = (n, m)$ with spin σ , and δx and δy are the unit vectors along the x and y directions. $\varepsilon_{\mathbf{i}}$ is the on-site energy, which is set to 0 everywhere for the clean system. When the center region is a disorder system, $\varepsilon_{\mathbf{i}}$ is set by a uniform random distribution $[-W/2, W/2]$. Here $t = \hbar^2/(2m^*a^2)$ is the hopping matrix element with the lattice constant a , \mathbf{I} is a two-dimensional identity matrix. The strength of Rashba SOI is represented by $V_R = \alpha\hbar/2a$, where α is the Rashba spin-orbital coupling. V_R is set to zero in the lead-2 and lead-4.

Considering a small temperature gradient $\Delta\mathcal{T}$ on the longitudinal lead-1,3, we can set the temperatures $\mathcal{T}_1 = \mathcal{T} + \Delta\mathcal{T}/2$, $\mathcal{T}_3 = \mathcal{T} - \Delta\mathcal{T}/2$, $\mathcal{T}_2 = \mathcal{T}_4 = \mathcal{T}$. The charge current in lead- p can be written as $J_{pe} = e(I_{p\uparrow} + I_{p\downarrow})$ and the spin current is $J_{ps} = (\hbar/2)(I_{p\uparrow} - I_{p\downarrow})$. Here $I_{p\sigma}$ is the particle current in lead- p with σ equals to \uparrow or \downarrow . $I_{p\sigma}$ can be obtained by the LB formula:^{9,10}

$$I_{p\sigma} = \frac{1}{\hbar} \sum_{q \neq p} \int dE T_{p\sigma,q}(E) [f_p(E) - f_q(E)] \quad (2)$$

where $T_{p\sigma,q}(E)$ is the transmission coefficient from the lead- q to the lead- p with spin σ and E is the energy of the incident electron. $f_p(E)$ is the electronic Fermi distribution function of the lead- p .

The spin Hall current in lead-2 and lead-4 can be calculated with the closed boundary condition in both lead-1,3 and lead-2,4, i.e. $V_1 = V_3 = 0$ and $V_2 = V_4 = 0$. From symmetry of the system, we know that $J_{2s} = -J_{4s}$.⁹ After the Taylor expansion, the spin Nernst coefficient $N_s \equiv J_{2s}/\Delta\mathcal{T}$ can be reduced to:

$$N_s = \frac{1}{4\pi} \int dE (\Delta T_{23} - \Delta T_{21}) \frac{E - E_F}{k_B \mathcal{T}^2} f(1 - f), \quad (3)$$

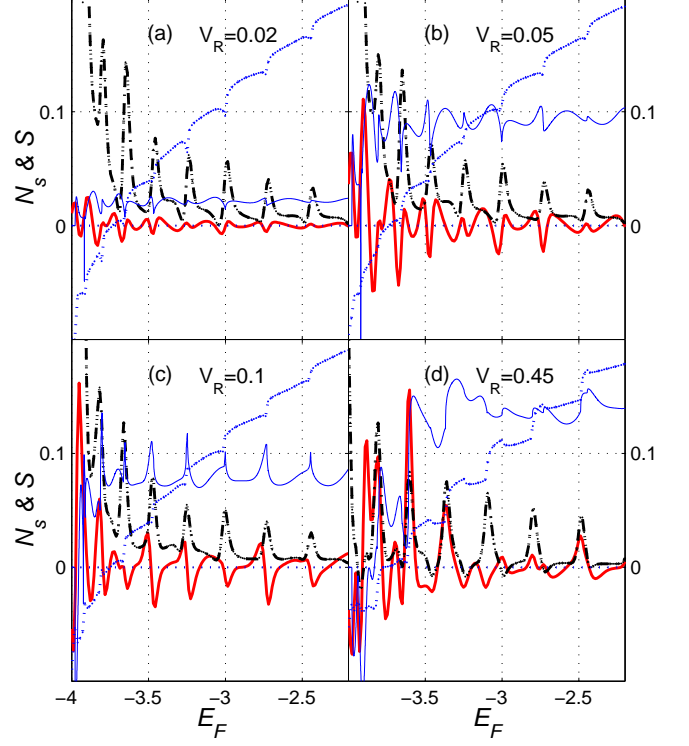


FIG. 2: N_s (red solid) and S (black dotted) vs. Fermi energy E_F for different Rashba V_R . The (scaled) transmission coefficient $T_{1,2} + T_{1,3}$ (thin blue dashed) and spin transmission coefficient $\Delta T_{2,3}$ (thin blue solid) are also shown. The other parameters are $\mathcal{T} = 0.01$, and $L = 19a$.

here $\Delta T_{2p} = T_{2\uparrow,p} - T_{2\downarrow,p}$, and f is the zero order of Taylor expansion of the Fermi distribution function, it is the same for all four leads, $f(E) = 1/\{\exp[(E - E_F)/k_B \mathcal{T}] + 1\}$.

For the calculation of the longitudinal seebeck coefficient S , we need the open boundary condition at lead-1,3, i.e. $J_{1e} = J_{3e} = 0$ to find the difference $\Delta V = V_1 - V_3$. Different from a quasi-one-dimensional 2-leads system¹¹, the extra leads-2,4 also affects the longitudinal seebeck coefficient S of the entire system. For example, with a perpendicular magnetic field B , the longitudinal seebeck coefficient S is affected by the bias in leads-2,4, V_2 and V_4 . However, without B , the sample's symmetry increases from C_2 symmetry to D_2 symmetry, i.e., we have $T_{1,2} = T_{1,4}$. Here $T_{1,2} = T_{1\uparrow,2} + T_{1\downarrow,2}$. After the Taylor expansion, we can get the longitudinal seebeck coefficient $S \equiv -\Delta V/\Delta\mathcal{T}$ as:

$$S = \frac{1}{\mathcal{T}} \frac{\int dE (T_{1,2} + T_{1,4} + 2T_{1,3}) (E - E_F) f(1 - f)}{\int dE (T_{1,2} + T_{1,4} + 2T_{1,3}) f(1 - f)}. \quad (4)$$

The equation above shows that, even with a higher symmetry, the longitudinal seebeck coefficient S is still affected by the transport properties from lead-2 and lead-4.

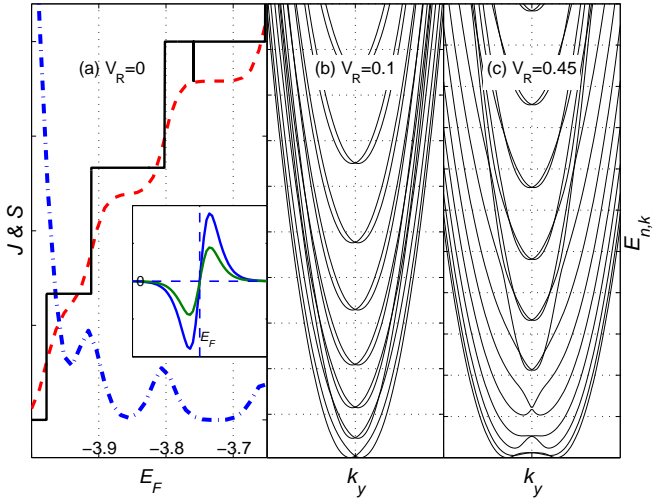


FIG. 3: (a) A simple model: Current J because of voltage gradient (red dashed) and thermal power S because of thermal gradient (blue dotted) vs. Fermi energy E_F at a two-lead system with Rashba $V_R = 0$. The (scaled) transmission function $T_{1,3}$ is also shown (black solid). The plot in the small box shows $f_L - f_R$ with temperature difference. (b) and (c): the eigen energy of the lead E_{n,k_y} v.s. longitudinal wave vector k_y (units: $1/2a$) for different V_R

With the D_2 symmetry, the relationship between S and N_s can be further derived. In fact, we can rewritten $S = (A^\downarrow + A^\uparrow) / [\int dE F(\varepsilon) (a^\uparrow + a^\downarrow)]$. The D_2 symmetry gives $\Delta T_{23} = -\Delta T_{21}$. Noticing $T_{3\uparrow,1} = T_{3\downarrow,1}$, the spin Nernst coefficient can be simplified as $N_s = (A^\downarrow - A^\uparrow) / (2\pi k_B T)$. Here $\varepsilon = E - E_F$ and $F(\varepsilon) = f(1 - f)$, a^\uparrow denotes the spin up term: $a^\uparrow = T_{2\uparrow,1} + T_{3\uparrow,1}$, and a^\downarrow the spin down term $a^\downarrow = T_{2\downarrow,1} + T_{3\downarrow,1}$, we also use the notation of the integral term $A^\uparrow = \int dE \varepsilon F(\varepsilon) a^\uparrow / T$ and $A^\downarrow = \int dE \varepsilon F(\varepsilon) a^\downarrow / T$. Because of the symmetry, only leads-1,2,3 are used in the simplified expression of S and N_s , we only need the upper half of the sample for our investigation. In fact, a^\uparrow (a^\downarrow) and A^\uparrow (A^\downarrow) reflects transport properties of spin-up (spin-down) electrons in the upper half of the sample. Roughly speaking, S can be seen as the sum of spin-up and spin-down terms, while N_s as the difference of them.

In the numerical calculations, $t = \hbar^2 / (2m^*a^2)$ is set as the energy unit. If taking the effective electron mass $m^* = 0.05m_e$ and the lattice constant $a = 12.5nm$, t is about $5meV$. Temperature is fixed by $k_B T = 0.01t$, which is about $1K$. The size of center region is $L = 19a$, about $237nm$. In a reasonable experimental range thus far $V_R \in [0, 0.1]$ ¹². However, in order to thoroughly study the relationship between the spin Nernst coefficient N_s and the seebeck coefficient S , we extend the range of V_R up to $[0, 1]$ in our calculation.

Fig.2 shows the spin Nernst coefficient N_s and the seebeck coefficient S versus the Fermi Energy E_F in the clean system ($W = 0$). It is clearly seen that the see-

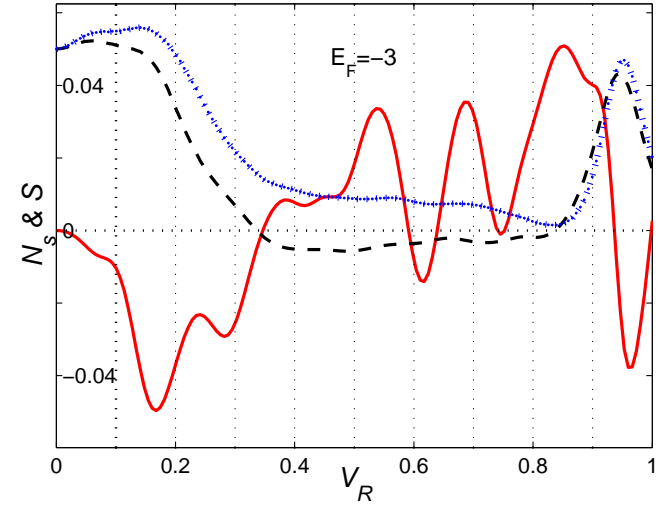


FIG. 4: (N_s (red solid) and S (black dashed) vs. Rashba SOI V_R for fermi energy $E_F = -3$. For compare, the blue dotted line shows the seebeck when lead-2,4 have the same V_R as lead-1,3. The other parameters are $T = 0.01$, and $L = 19a$.

beck coefficient S peaks at the positions where there are step-changes of transmission function $T_{1,2} + T_{1,4}$. These peaks can be explained by a simple model only with a 2-lead system without the Rashba SOI, shown in Fig.3(a). The transmission coefficient $T_{1,3}$ is a step function (solid-black curve). The reason is as follows. The sample can be considered as a multi-channel system at a low temperature (here $T \sim 1K$). When fermi energy increases, more channels in the lead are used to transport current. Thus, ΔV of two leads as well as the current increase with increasing of fermi energy (red-dashed curve). However, the S (blue-dotted curve) can not accumulate while E_F increases, it only peaks while the channel number changes and S is close to zero with a fixed channel number. This can be seen from the LB formula (2), if lead-p and lead-q have different temperatures, $f_p(E, T + \Delta T) - f_q(E, T - \Delta T)$ is an antisymmetry function of $E - E_F$ (see plot in small box of Fig.3(a)): when $E < E_F$, $f_p < f_q$, current flows from lower temperature lead to higher temperature one; when $E > E_F$, current flows in the opposite direction. Only when the two flows are not equal, i.e. $T_{p\sigma,q}$ has an antisymmetry part, we can have a nonzero current. Thus for Fig.3(a), only when $T_{1,3}$ is at the step-change point, it has antisymmetry part and can give a non-zero S .

This conclusion can also be used to analyst spin-involved quantities. From Fig.2, we can see that N_s (red solid line) shows an oscillatory structure. Besides the peaks at $V_R = 0$ (N_s is zero at this point), the magnitude of N_s oscillation is also large at the peaks of S ; but at the exact maximum point of S , where V_R is quite small ($V_R \lesssim 0.1$), N_s is generally close to zero. This is because the spin transmission coefficient $\Delta T_{2,3}$ generally has an extreme value when the transmission coefficient

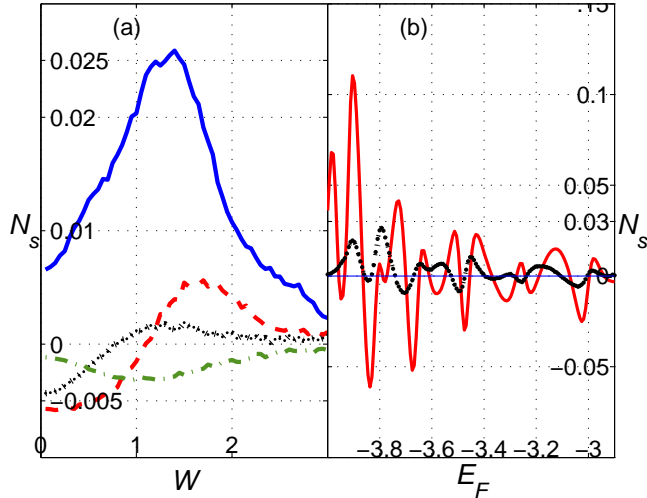


FIG. 5: (a). N_s vs. the strength of disorder W for different Fermi level $E_F = -3.8$ (solid blue), $E_F = -3.6$ (dashed red), $E_F = -3.0$ (dotted black), $E_F = -2.2$ (dotted dashed green); (b). N_s vs. Fermi energy $E_F = -3.8$ for $W = 0$ (dashed black) and $W = 1.4$ (solid black).Other parameters are $V_R = 0.05$, $\mathcal{T} = 0.01$, and $L = 19a$.

jumps at a step. Around an extreme value, any function is almost symmetry, thus one only can get a low value of N_s . While at both sides of the extreme value, $\Delta T_{2,3}$ monotonically increases or decreases, we can get a local maximum magnitude of N_s . Now why $\Delta T_{2,3}$ has an extreme value at a peak of S for a small V_R . Due to the Rashba SOI, each eigen-energy band splits into two sub-bands with opposite spin directions. These two sub-bands degenerate at $k_y = 0$, and the lower sub-band has two valleys below this degenerate point. The two sub-bands are very close to each other when V_R is small. If the lower sub-band of high level (for example, E_{1,k_y}) has the similar spin direction with the upper sub-band of low level energy (for example, E_{0,k_y}), $\Delta T_{2,3}$ continually increases when E_F goes from the upper band of E_{0,k_y} to the two valleys of lower sub-band of E_{1,k_y} , and then rapidly decreases when E_F goes through the degenerate point ($k_y = 0$) of E_{1,k_y} , thus we get a peak in $\Delta T_{2,3}$; otherwise we get a valley in $\Delta T_{2,3}$.

When V_R is very big, we can see the external peaks for both N_s and S . For example $V_R = 0.45$ in Fig.2(d), close to the 2nd and 3rd main peaks of S , we can see a very sharp sub-peak of N_s . In fact, these are also the small peaks of S , though not very big. This is because for these two band (see Fig.3(c)), the two valleys of the lower sub-band is far from the degenerate point at $k_y = 0$, the two channel of these two sub-bands is separated. Thus we can see two peaks. At this time, the change of spin transmission coefficients can be roughly thought as the change of transmission coefficients, thus we can see N_s peaks at the S 's peak.

In Fig.4, we show the spin Nernst coefficient N_s and

the seebeck coefficient S versus the Rashba SOI V_R in the clean system ($W = 0$) for $E_F = -3$. The seebeck coefficient S decreases and maintains for a small value for quite a while before shows another peak. This is because increasing V_R moves the energy bands and makes them go through the fermi energy. It should be mentioned that we found the negative seebeck coefficient S (Fig. 2d), which means a longitudinal current occurs in the opposite direction of the temperature gradient $\Delta\mathcal{T}$. This is due to the boundary conditions $V_R = 0$ at leads-2,4. As a compare, we also show S for a uniform system, i.e. leads-2,4 having the same strength of V_R as in the sample. For this situation, the seebeck coefficient S is no longer negative. In fact, when the Rashba SOI is absent in the leads-2,4, an interface between $V_R = 0$ and $V_R \neq 0$ occurs⁹, this interface causes additional scattering for an incident electron. In some special case like $E_F = -3$, this may make the electrons below E_F easier to transport than the electrons above E_F , thus a negative S .

Finally we discuss the disorder effect on the spin Nernst effect. Fig.5 shows N_s versus disorder strength W for different Fermi energies. The calculations are averaged over 500 disorder configurations. Around $W < 1.7$, N_s shows an oscillatory structure. N_s changes sign with increasing of the disorder strength (see $E_F = -3.6$ and -3.0 in Fig.5). It is interesting to see that, comparing to a clean system ($W = 0$), N_s can be unexpectedly increased by disorder W . This is because the disorder changes the oscillating structure of N_s (see Fig.5b). As expected, the disorder decreases the strength of oscillating, however, it also shifts the peak positions of N_s . It is possible to have a peak in N_s at finite disorder while it is almost zero initially at clean limit. In Fig.5a, around $W = 1 \sim 1.5$, for the Fermi level $E_F = -3.8, -2.2$, we can see that N_s is up to about three times of N_s at $W = 0$. The behavior of N_s v.s. W is very apparent when the Fermi level E_F is close to the bottom of energy band ($E_F = -4$). For $E_F = -3.8$, N_s is much bigger than those at other Fermi levels, and we can see a very remarkable peak at about $W = 1.4$. For $E_F = -2.2$, N_s begins from -0.005 , changes its sign at about $W \sim 1.25$ and than increases, again reaches to 0.005 at about $W \sim 1.75$. With a very big disorder, N_s should go to zero as system enters into an insulating regime. We find that the zero of N_s occurs at $W = 3$ for $V_R = 0.05$. This is roughly independent of the locations of the Fermi energy.

In summary, in the absence of a perpendicular magnetic field, the interplay between the spin Nernst effect and the seebeck effect is investigated in a two-dimensional cross-bar with a spin-orbit interaction. The spin Nernst effect exhibits an oscillatory structure for a wide range of the Rashba SOI. With a large Rashba SOI, the N_s oscillation has a peak when the seebeck coefficient possesses one. However, the inverse condition is not always satisfied, namely, the seebeck coefficient can be almost zero while N_s has a peak. The disorder effect on the spin Nernst effects is also studied. We find that disorder can enhance N_s up to three times for some

Fermi levels. In addition, the disorder can also change the sign of spin Nernst effect. Moreover, the limit of disorder where N_s goes to zero is independent of the Fermi energy.

Acknowledgments: We thank Q.F. Sun and S.G. Cheng for many helpful discussions. We gratefully acknowledge the financial support from US-DOE under DE-FG02-04ER46124 and US-NSF.

^{*} Electronic address: xuele@okstate.edu

² A.S. Dzurak, *et al.*, Phys. Rev. B **55**, R10197 (1997); R. Scheibner, *et al.*, Phys. Rev. Lett. **95**, 176602 (2005); Phys. Rev. B **75**, 041301 (2007).

³ L.W. Molenkamp, *et al.*, Phys. Rev. Lett. **65**, 1052 (1990).

⁴ A.A. Abrikosov, *Fundamentals of the theory of metals* (NorthHolland Amsterdam, 1988).

⁵ J.M. Iiman, *Electrons and phonons* (Oxford university Press, Oxford, U.K., 1960).

⁶ C.W.J. Beenakker and A.A.M. Staring, Phys. Rev. B **46**, 9667 (1992).

⁷ H. Nakamura, N. Hatano, R. Shiraishi, Solid State Communications **135** (2005); R. Shiraishi, H. Nakamura, N. Hatano, J. Surf. Sci. Nanotech. Vol. **3**, 518 (2005).

⁸ K. Behnia, *et al.*, Phys. Rev. Lett. **98**, 166602 (2007); Science **317**, 1729 (2007).

⁹ Shu-guang Cheng, Yanxia Xing, Qing-feng Sun, and X. C. Xie, Phys. Rev. B **78**, 045302 (2008).

¹⁰ L. Sheng, D. N. Sheng, and C. S. Ting, Phys. Rev. Lett. **94**, 016602 (2005); W. Ren, *et al.*, Phys. Rev. Lett. **97**, 066603 (2006); Z. Qiao, J. Wang, and H. Guo, Phys. Rev. Lett. **98**, 196402 (2007); Y. Xing, Q.-F. Sun, and J. Wang, Phys. Rev. B **75**, 075324 (2007).

¹¹ M. Cutler and N. F. Mott, Phys. Rev. Lett. **88**, 136601 (2002).

¹² T. P. Pareek, cond-mat/0412115v2; Takaaki Koga, *et al.*, Phys. Rev. Lett. **89**, 046801 (2002); G. Engels, *et al.*, Phys. Rev. B **55**, R1958 (1997).

¹³ H. Jiang, L. Wang, Q.F. Sun, and X.C. Xie, to appear in Phys. Rev. B (arXiv:0905.4550).